Electronics and Electrical Engineering

AIMS Electronics and Electrical Engineering, 6(2): 161–177.
DOI: 10.3934/electreng.2022010
Received: 26 December 2021
Revised: 11 April 2022
Accepted: 18 April 2022
Published: 20 April 2022

http://www.aimspress.com/journal/ElectrEng

Research article

Peculiarities of the radiated field in the vicinity of a mobile terminal connected to 4G versus 5G networks during various applications usage

Simona Miclaus[1,*], Delia-Bianca Deaconescu[2], David Vatamanu[1], Andreea Maria Buda[3], Annamaria Sarbu[1] and Bogdan Pindaru[1]

[1] Department of Communications, IT & Cyber Defense, "Nicolae Balcescu" Land Forces Academy, Sibiu, Romania
[2] Doctoral School of Electrical Engineering, Technical University of Cluj-Napoca, Cluj-Napoca, Romania
[3] Faculty of Electronics and Telecommunication, Politehnica University, Bucharest, Romania

* **Correspondence:** Email: simo.miclaus@gmail.com; Tel: +40 269432990.

Abstract: Realistic human exposures to radiation emitted by a mobile terminal connected to either a 5G network (sub-6 GHz) or to a 4G network have been scarcely assessed till now. Present experimental work aimed at comparing the radiated field in air, in a single point situated at 10 cm from a mobile phone when running a set of 5 mobile applications in the two communication standards. The time-evolution of the electric field strength in air near the terminal during 25 s of use was recorded by an original method, together with the data rate of transmission. The emitted power density dynamics, its statistics, its slope of accumulation after the usage period and its average value per transmitted bit are analyzed and compared between all the situations. The peculiarities are emphasized and they are proved to depend on the communication standard and on the mobile application.

Keywords: 5G mobile phone; human exposure; microwaves; mobile applications; sub-6GHz networks

1. Introduction

Recently, the mobile communications evolved from the 4th generation (4G) which uses Long Term Evolution (LTE) standard of communications, to the 5th generation (5G), whose radio access uses an air interface called 5G New Radio (5G NR). 5G networks are today deployed in the majority of the countries in their first stage, using sub-6 GHz band, overlapping frequencies sometimes with 4G networks. 5G NR technology uses two different frequency ranges: Frequency Range 1 (FR1) [1] – with frequencies not exceeding 6 GHz plus an extension up to 7.125 GHz, and Frequency Range 2 (FR2) [2], which covers the range (24.25–52.60) GHz. In the 3rd Generation Partnership Project (3GPP) technical standard TS 38.101 [3], tables with specified frequency bands and the channel bandwidths of the 5G NR standard are provided. NR bands are defined with prefix "n". When the NR band is overlapping with a 4G LTE band, they share the same band number.

The electromagnetic exposure (EME) of a person during the use of the mobile terminal for various voice or data applications remains one of the challenging aspects to investigate, especially in the 4G and 5G networks, due to the very high variability of the emitted signals in time and in space [4–7]. The frequency and the proximity of the UE to the body are important in connection to the treatment of the near- or far-field conditions of EME. For sub-6 GHz frequency range, the EME compliance is assessed using specific absorption rate (SAR) of energy deposition in the tissues, while for frequencies exceeding 6 GHz, the power density (incident, in air, or absorbed – in the skin) [8,9] is used. An overview of the newest EME compliance assessment procedures and measurement techniques applicable to the 5G NR FR2, above 6 GHz for incident power density are provided in IEC TR 63170 [10].

Beyond the procedures officially implemented for 5G measurements, interesting research approaches come to supplement the knowledge. The basic principle used for the exposure assessment in the past 2G, 3G, and 4G technologies was to measure the power received from a constant radio frequency source (a pilot signal) and then to apply a proper extrapolation factor. This kind of approach cannot be purely translated to 5G technology, because 5G NR uses a completely different philosophy: flexible numerologies, advanced Time Division Duplexing (TDD) and spatial multiplexing techniques (beam sweeping and Massive Multiple Input Multiple Output (MIMO)). Therefore, authors of [11], proposed an extrapolation technique based on taking into account the effects of the TDD and of the sweep beam to assess the instant maximum power received. Moreover, they explored the possibility of using a beam-forcing technique of the user equipment (UE) [12], assigning the terminal an active role and forcing it to take over the most suitable configuration. They concluded that a key point in the measurement procedure is the use of a mobile phone able to actively interact with the base station (BS), otherwise measurements are performed in unknown radiation beam states. With the use of Multi User-MIMO the complexity of the measurement will increase even more by increasing the number of possible states in terms of pattern configurations. Using mobile terminals that can actively interact with the BS would force some specific states suitable for the measurement, so the procedure of field level assessment can be tailored properly. Another recent research work followed the development of a protocol for the determination of auto-induced exposure of both a user's own devices and the networks' BSs, making use of a personal exposure meter and a mobile device connected to the 5G NR network [13]. This type of problem is indeed very indicative, since massive multiple-input multiple-output (MaMIMO) antenna arrays with intelligent precoding schemes are implemented in 5G [14]. The precoding scheme aims to maximize

the signal strength at the intended user and sometimes to minimize it at unintended users (spatial multiplexing) in the downlink. When the intended user is in the line of sight (LOS) of the BS, a narrow beam towards the user is forming. When LOS is obstructed a hotspot appears at the UE location because more than one dominant path between BS and UE exist [15]. Multiple paths can constructively interfere and the UE is found in a temporary hotspot area. The MaMIMO technique improves the signal-to-noise ratio by updating the precoding in real-time while the users are moving, changing their positions. The channel state is continuously updating the information between the BS and the UE by the pilot tones transmission. Therefore, the complexity and dynamics of the local EME is extremely high.

Besides approaching procedures, a series of papers analyzed, by simulation or by measurement, the compliance of the exposure levels due to 5G UE usage. For example, in [16] authors checked the maximum permissible transmitted power and the maximum equivalent isotropically radiated power of FR2 terminals by numerical modelling of patch antenna arrays of different sizes (ranging from 2 × 2 to 16 × 16) and of a variety of array topologies, taking into consideration possible beam-steering operations. In [17] the time-averaged output power of several UEs operating in two real commercial 5G FR1 networks was measured over fifteen days by means of a network management platform and a very conservative assumption in the applied method was implemented. In TDD situation it was found that the time-averaged output power of the terminals was less than 43% of the maximum time-averaged output power and 95% of the time-averaged power samples recorded were less than 8% of the maximum, while the mean value was less than 2%. To take into consideration the EME, a new planning method of a 5G cellular network was also proposed and discussed [18], in which all three criteria were considered together: next-generation Node-B (gNB) installation costs, 5G service coverage level of MIMO, and the integrated restrictive EME constraints.

On the other hand, EME assessment in the near-field of a UE is a very complex task and scarce literature exists on the subject. It was approached in [19] and [20], where a technique based on source reconstruction was applied for FR2 band terminals. The results showed that the measured and simulated power density agrees well even at evaluation planes situated at one fifth of a wavelength ($\lambda/5$) away from the UE. In [21] and [22] a fast power density assessment method for 5G FR2 handsets was proposed and checked, using the equivalent currents. It allows determination of the power density with acceptable accuracy in close proximity of a UE.

Other recent papers were devoted to numerical modelling of EME of 5G user head in connection with compliance checking [23–29], or to the issue of designing antennas [30,31] including ones to enable the decrease of exposure [32,33]. Even research on the identification of materials with very good shielding properties emerged [34]. Complementary research directions were also developed in the last couple of years. In one paper the relations between temperature rise, SAR and incident power density were identified, for the case when brain tissue is radiated either by continuous wave at very low power or by rapid pulse sequences and single pulses with varying pulse duration [35]. The beam penetration, absorption and thermal diffusion were also assessed. Furthermore, another work [36] highlighted thermal responses of skin to pulsed millimeter waves, demonstrating that implicit limits on pulse fluence are not protecting against some class of emissions (of nonlethal weapons) in the same frequency range of 5G communications. An analysis of the risk of higher EME in case of narrow beams used in 5G communications is provided in [37] which argues that localization-enhanced pencil beamforming conducts to an important reduction of UE exposure if compared with fixed width beams.

User exposure was scarcely assessed experimentally in real life conditions and at least in 5G networks no paper has been identified on the subject. Present work aimed at an experimental assessment of the dynamics of the radiated field in a point in air, nearby a terminal, when different mobile applications run on the phone. The peculiarities of EME are emphasized and differences between emitted field time-variabilities are followed comparatively for 4G network and for sub-6 GHz 5G network connections. In the investigated case, no beamforming was emitted by the terminal at the 5G connection, and the bandwidth in 5G was low, of 40 MHz, restricting the data rate of transmission to values not very much larger than in the 4G standard. The main focus was on quantification of the time-variability corresponding to the emission while the phone was running some types of usual mobile applications. The main reason of this approach was to underline the differences between the time-prints of emitted powers by the phone when it uses one or another communication standard or respectively when different mobile applications are used. Practically, the new metrics used here provides the rate of power density accumulation in time and the power density emitted per transmitted bit. The time profile of mobile usage is valorized in this way, fact that is crucial in new 5G philosophy. The rest of the paper is organized in the following way: the second section describes the measurement set-up based on small field probes and real-time spectrum analyzers that provide the channel power calculation at every 100 ms. In the third section the time- and frequency peculiarities of the emissions during 25 s are emphasized for five different mobile applications in the two communication standards. The fourth section show the statistics of post-processed data and establishes clear differences based on the new introduced quantities: a) power density rate of accumulation during phone's usage in different real-life usage situations and b) emitted power density per transmitted bit corresponding to 4G and 5G standards.

2. Measurement set-up and procedure

In the present work we have experimentally investigated the electric (E)-field strength variation in time nearby a UE connected to one of the two networks: a) 4G LTE, using a channel bandwidth BW1 = 20 MHz at a central frequency f1= 2.59 GHz and time division duplexing (TDD); b) 5G NR FR1 in the band n77, at f2 = 3.7 GHz, using C band, which covers both uplink and downlink in the range 3.3–4.2 GHz, with a channel bandwidth BW2 = 40 MHz in TDD. 5G NR FR1 offer bandwidths from 10 MHz up to 100 MHz, but during our measurements the bandwidth was always of 40 MHz.

A Motorola smartphone model Moto g 5G plus (XT 2075-3) was used as a UE (3 GPP power class 3, handheld UE). It provides a maximum transmitted power of 23 dBm in both 4G and 5G bands. In Figure 1 (left) a picture of the uncovered back side of the phone is provided, where the emitting antennas are observed. The phone was connected to base stations antennas situated at cca. 75 m away, in non-line-of-sight conditions (UE inside a building).

The measurement equipment was composed of a set of three identical portable real-time spectrum analysers and respectively three miniature E-field probes (sniffers). The probes were equally distanced in-between and positioned at a distance d = 10 cm from the phone's back surface (Figure 1, right). We used a spectrum analyser Spectran 5 (Aaronia) model HF 80120 V5 X, and a PSB E1 near-field probe model (Aaronia). Two software packages were used to display and record the data as received spectrum (in dBm) versus time: Aaronia RTSA Suite Pro and Aaronia MCS Spectrum Analysis. An original Android application developed initially for WiFi communications [36] by part of the authors of present paper, was adapted here for the mobile network to measure the data

rate of transmission simultaneously with the recorded signals emitted by the UE. The mobile application was configured to operate with all mobile networks, but to discriminate between 4G and 5G ones. The sample rate was 100 ms for both the signal spectrum recordings and for the data transfer rate recordings. The synchronization between the instruments measuring the E-field level and the phone running the Android application for data rate determination [38] was not always reliable enough, so that statistics of the data was applied in the post-processing step to provide the overall results. We considered that data rate value is one of the major influencers of the exposure level and its knowledge is significant [39]. The averaging over data rate values was made here taking the three sets of recordings at each of the probes P1, P2 and P3, recordings called R1, R2, R3 (they were repetitions). Each E-field and data rate recording lasted 25 s. The settings of the analysers were: real time bandwidth span (RTBW) = 88 MHz (for 4G) and 44 MHz (for 5G), step = 1MHz, Bins = 896.

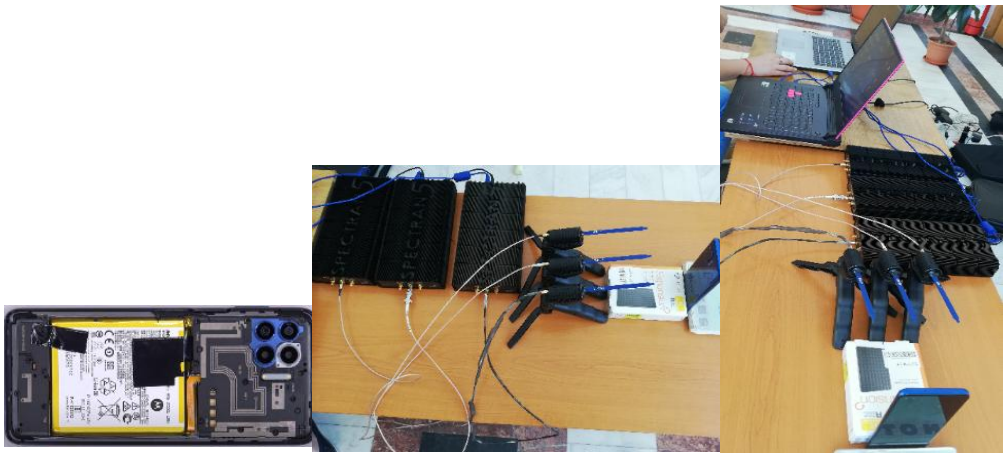

Figure 1. The measurement set-up composed of field probes and real time spectrum analysers connected to the laptops, and the interior of the Motorola One 5G phone, to observe the positions of the antennas dimension.

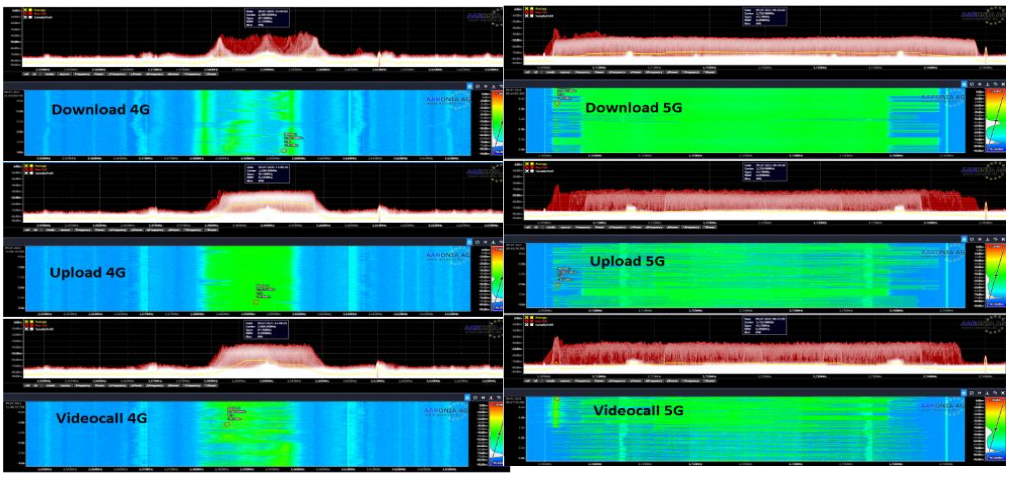

Figure 2. View of the representations given by Aaronia RTSA Suite Pro for the spectrum and spectrogram, of the signals emitted by the phone when three applications are running: file download, file upload and Video call on WhatsApp.

Five mobile applications were used as sources of field emissions during monitoring of 25 s long, for both 4G and 5G connections: file download, file upload, streaming, video call and voice call. The spectrum and spectrograms of three of the applications' emitted fields (as captured by one of the probes) are represented in Figure 2, during a couple of seconds. In Figure 2 – left, the 4G applications are showed, in Figure 2 – right, the similar application in the 5G band are showed.

The raw data were constituted by the recordings sets of the spectra captured every 100 ms. Practically 250 spectra in the transmission channel formed the initial database per each case. From one spectrum we then calculated the channel power, P_{ch}, by using the summation formula:

$$P_{ch} = \frac{\sum_{f=Freq.\ start}^{Freq.\ stop} 10^{\frac{FFT\ \ Bin\ (f)}{10}}}{Window\ \ bandwidt\ h} \tag{1}$$

where Freq. start and Freq. stop are the limits of the spectrum in the occupied channel, FFT Bin(f) is the power level (in dBm) of each of the spectral components (we had 440 frequency bins) and window bandwidth is the resolution bandwidth (in our case it was of 195 kHz for the 4G measurements and of 98 kHz for the 5G measurements).

Then, P_{ch} (in mW) was transformed in E-field strength value by using the calibration files of the E-field probes.

Finally time series of E-field strengths values were obtained for each of the 4G or 5G bands (of 20 MHz and 40 MHz respectively) and for all mobile applications emissions. Overall, one tandem of E-field level (in V/m) and data rate (in Mbps) were the strings in time provided every 100 ms.

3. Time and frequency behavior of the channel while running mobile applications in 4G versus 5G networks

Tri-dimensionally representations of the distribution of power versus frequency and versus time (3D spectrograms) were obtained from the matrix of data (440 columns of frequency data x 250 lines of time data). To emphasize the differences between 4G and 5G applications, we rotated the 3D graphs so as to better observe in a plane either the time-evolution profile (Figure 3) or the frequency-evolution profile (Figure 4) during 25 s of each application running. Notable differences are observed with the necked eye between 4G and 5G situations. Time distribution of power spectra (Figure 3) indicate that the densest distribution belongs to upload in 4G, while the rarest belongs to streaming in 4G. Abscissa in Figure 3 is the time and ordinate is the channel power level. Frequency distributions of the accumulated power density in time observed in Figure 4 are indicative for unerlining the 20 MHz and 40 MHz respectively channels bandwidths and the variability of the levels in the band. Abscissa in Figure 4 is the frequency and ordinate is the accumulated power density (summation of 25 s contributions). These primary data were than post-processed to extract the significant quantities.

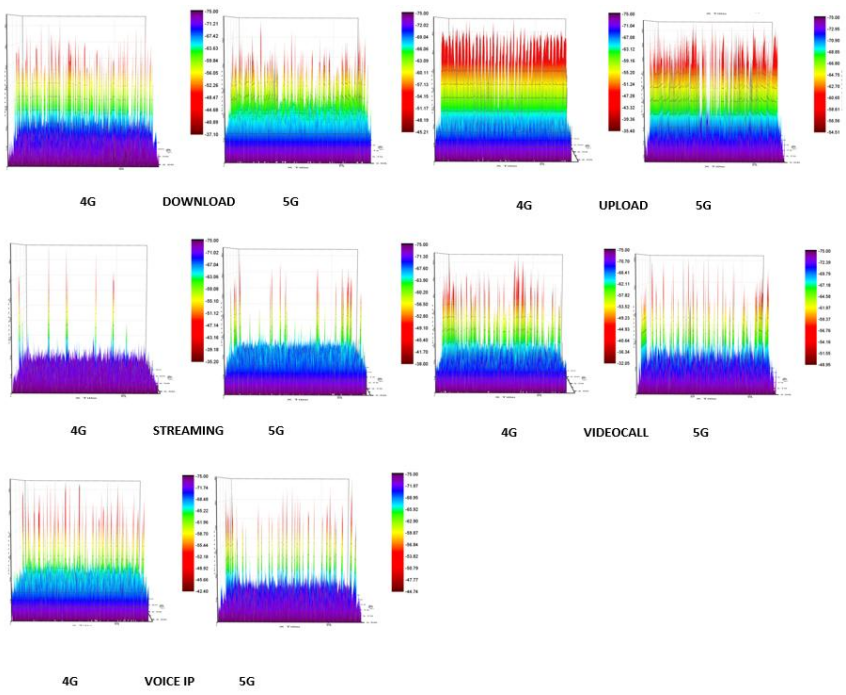

Figure 3. Planar representation of the channel power values distribution in time, emphasizing the time evolution of power levels during 25 s, comparatively 4G (left side) to 5G (right side) for each wireless application running.

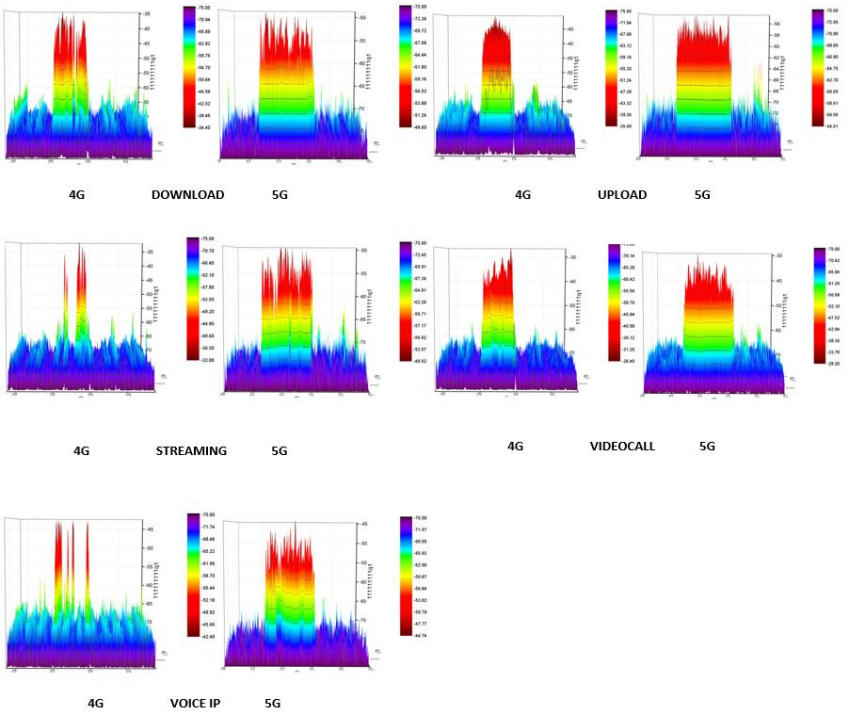

Figure 4. Planar representation of the channel power values accumulated in time in the channel bandwidth, emphasizing the spectral energy density during 25 s, comparatively 4G (left side) to 5G (right side) for each wireless application running.

4. Radiated field levels and data rates while running mobile applications in 4G versus 5G networks

Channel power values are not to be compared between 4G and 5G communications, since the calibration files of the probes in the two frequency bands differ, so we can compare exposure only if we use the final computed E-field strengths based on channel power determination.

E-field levels distributions over 25 s for each probe P1, P2, P3 and for each repetition R1, R2, R3 were computed. E-field strengths in the channel varied in time during 25 seconds, as exemplified for probe P1 in repetition R1 in Figure 5. We grouped representations for 4G and for 5G where all five mobile applications are superimposed. Similar results were obtained for the other probes and repetitions. For a better observation of dissimilarities, Figure 6 emphasizes sets of two time-variations of the same application running in 4G versus 5G network. Rare and ample spikes are present during video call and streaming in 4G, while in 5G network denser spikes are observed. Notable differences appear between the two communication standards during all applications usage. The most interesting differences may be noted during upload, streaming and voice call.

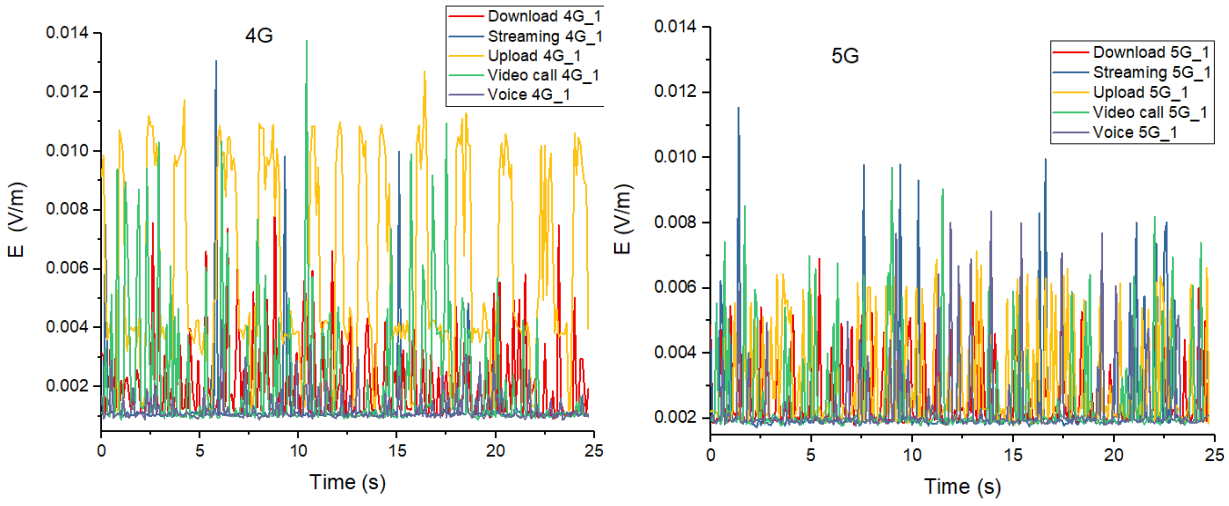

(a) **(b)**

Figure 5. The variation in time of the E-field in the channel, as measured by probe no.1, for the five applications running in: a) 4G network; b) 5G network.

Then, the boxplots of E-field strengths values distribution in time with figured outliers were obtained and used for comparison between applications in 4G and 5G networks. In Figure 7 the obtained E-field strengths distributions for field-probes P1 and P3 are exemplified. Interquartile intervals are largest during uploading files (most spread values), both in 4G and in 5G. Mean values (figured by the central rectangle) are largest for upload and lowest for voice call and streaming. Average emitted fields were generally higher with the phone connected to 4G than to 5G network, and the ratio could reach as high as 2.7 times (for upload). In Figure 8 the mean coefficients of variation of the E-field strengths are represented. It is concluded that larger variations of the signals are observed during 25 s while in streaming and in video call in both standards, but inter-standards the coefficient of variations are larger generally in the 4G emission.

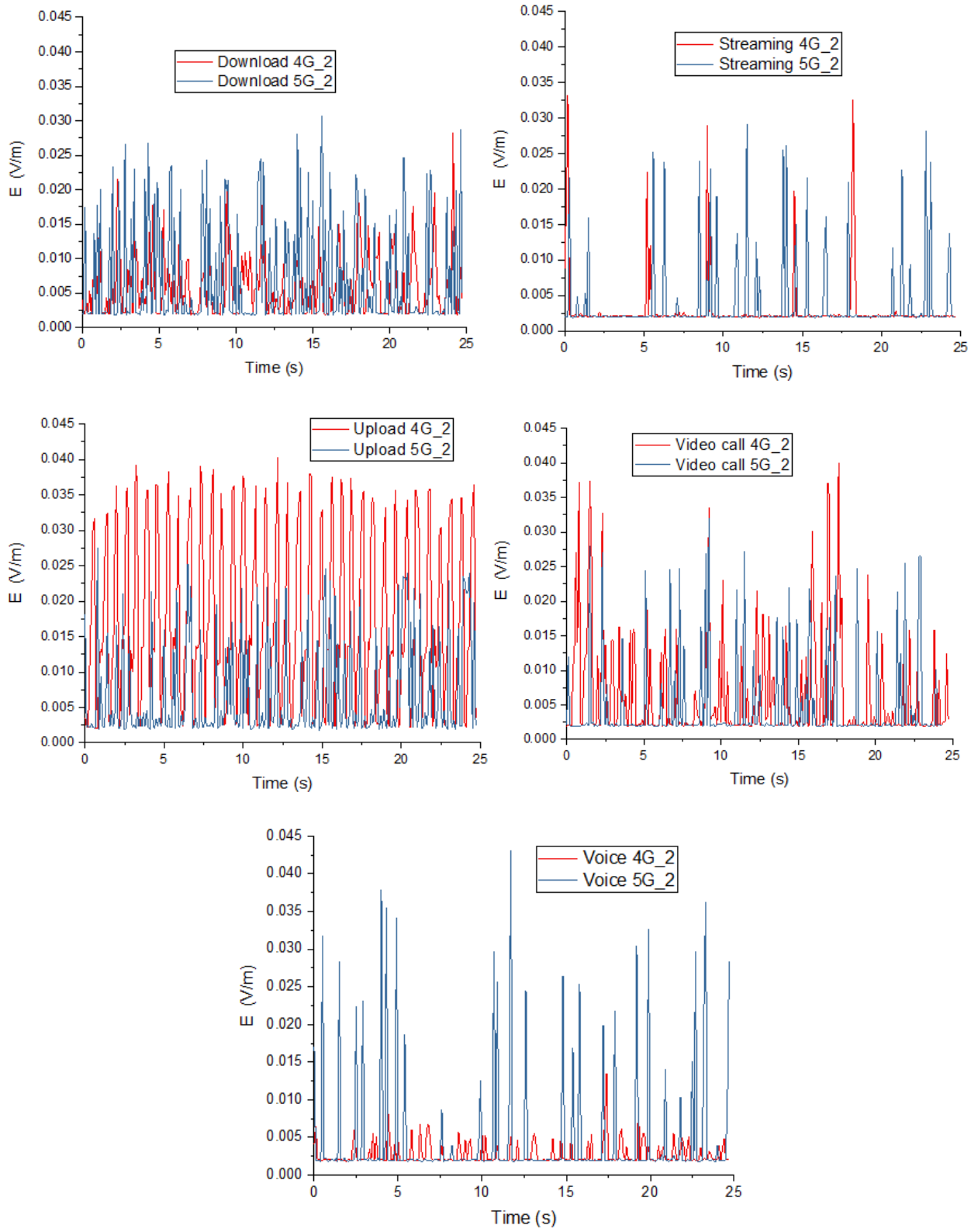

Figure 6. The time evolution of the E-field strengths in the communication channel during 25 s use of wireless applications, as captured by probe no. 2: 4G versus 5G peculiarities.

However, the significant differences are due to time distribution of the spikes in-between the two standards of communication, as already observed in Figure 5 and Figure 6. Therefore, we also represented the probability density functions (PDF) of the radiated E-field strengths distributions as observed in Figure 9. The following probability functions were identified for P1 example: a) in the 4G network: Log-logistic function for streaming and voice call; Inverse Gaussian function for download and video call; Gen. Pareto function for upload; b) in the 5G network: Pearson 5 (3P) function for download and upload; Dagum function for streaming; Log-Logistic (3P) function for video call, voice call. In order to better classify the distributions, larger databases are needed. For the time being, it seems that no notable differences appeared, with the exception of upload application.

Analysing the rates of data transfer (both the upload transfer speed and the download transfer speed), Figure 10 shows us the following: in the upload transfer speed case, except of the video call, all the applications run faster in 5G than in 4G, for example in case of file download the ratio of average speed is of 6 and in case of file upload the ratio is of 2. In the download transfer situation, the ratio between data transmission rates in 5G versus 4G is consistently larger than unit only in the case of file download, when the ratio coefficient is almost 5. We conclude that the investigated case was not very indicative: the data rates were not excessive different in the two standards, so the 40 MHz bandwidth in the 5G and the 20 MHz bandwidth in 4G network did not ensure considerably different speeds. This is due to the fact that the subscriber need one specific subscription type to the mobile operator, so that no reduction of speed to be applied during the use of traffic – case which it seemed to happen in the present UE experiment. So, in a real usage situation, in order to highlight specificities of 5G as compared to 4G links, one needs to receive much larger bandwidths and much higher speeds. In the present case, Figure 10 shows the data rate values distribution estimated by the boxplot representations which do not highlight impressive differences. We estimate that comparing for example a channel bandwidth of 20 MHz (in 4G, at central frequency of 2.59 GHz) with a channel bandwidth of at least 80 MHz (in 5G, at a central frequency of. 3.7 GHz), will provide more significant differences between average exposures also. As we have proved in an earlier paper [37], the exposure levels are influenced by the data transfer rate also, but this is not the only parameter that matters.

Based on E-field strengths strings of data, we then calculated the power density in air, considering the far-field formula. With the corresponding power density values, as exemplified in this paper for P1, we calculated then the accumulated power density evolution in time. Practically, in the point in air where the probe was situated, we calculated the rate with which the power density increased, as integrated in time during 25 s. The graphs of this integrated power density evolution are represented in Figure 11, comparatively between 4G and 5G emissions. As seen, much variable slopes of the curves appear in 4G, so the dependence on the application is much higher in this standard.

To observe the differences between the average slopes, we represented graphs in Figure 12a. Here, comparatively for the two networks we may see the average rate of power density accumulation in time (in W/m^2 per second), for each checked mobile application. It is seen that much different slopes belong to 4G application running than to 5G. In 4G, the highest rate of power density accumulation is attributed to upload of files activities, and its value is at least double than all other rates. In 5G, the rates are more similar, but still the upload conducts to the highest rate of accumulation. This integrated approach has been already used by us as an original one, in a previous paper [4]. Here we could apply this metrics to characterize the time-evolution of EME in 5G also, which we consider very important, besides stated exposimetry metrics generally applied in the field. In Figure 12b we show the calculated average power density emitted per bit, relating the average power density rate with the upload transfer

rate. As observed, the larger values belong this time, in both standards, to streaming. In all the cases however, lower power density rates corresponded to one transmitted bit in 5G than in 4G network. One step further, the mean energy density per transmitted bit can be also calculated, but proportional values would be achieved.

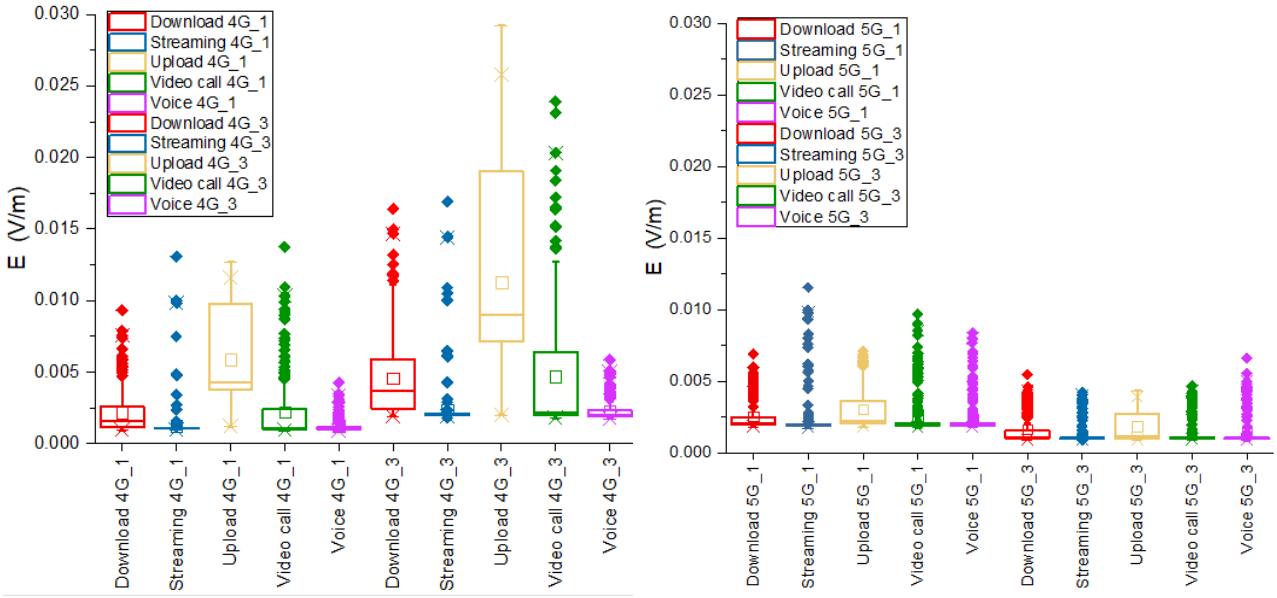

(a) **(b)**

Figure 7. Boxplots with outliers of the E-field strength distributions in the channel during 25 s use of various wireless applications: a) 4G channel of 20 MHz at 2.59 GHz; b) 5G channel of 40 MHz at 3.7 GHz.

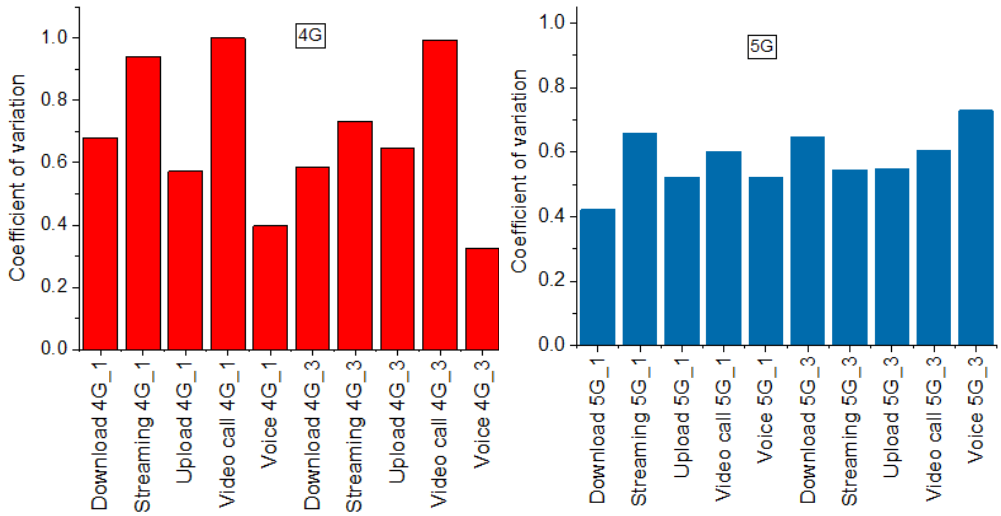

(a) **(b)**

Figure 8. Coefficient of variation of the E-field strength distributions for two of the probes (no. 1 and no.3) during 25 s: a) 4G channel of 20 MHz at 2.59 GHz; b) 5G channel of 40 MHz at 3.7 GHz.

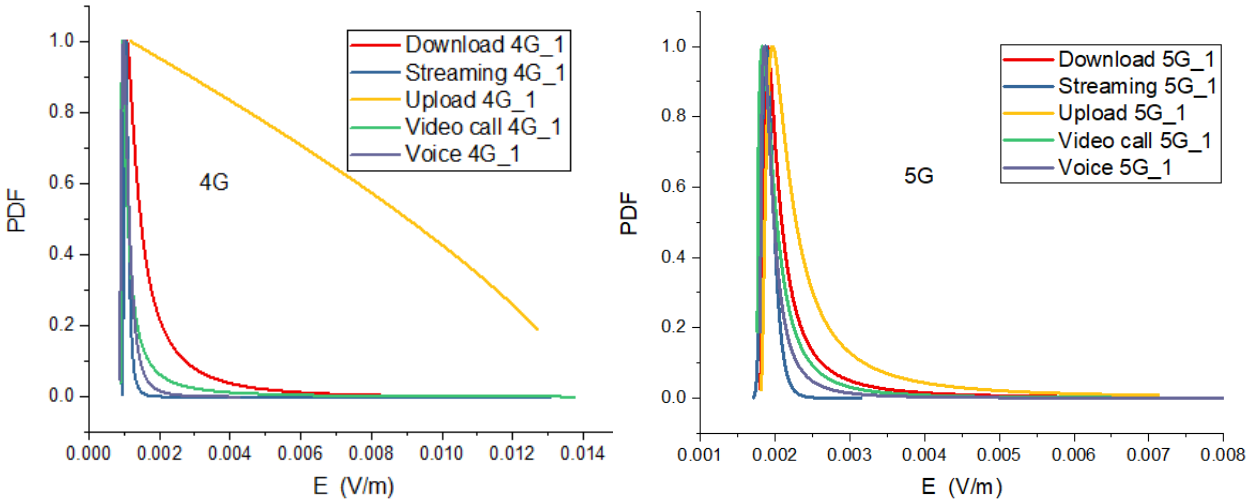

(a) **(b)**

Figure 9. Probability density functions of E-field level distributions: a) 4G channel of 20 MHz at 2.59 GHz; b) 5G channel of 40 MHz at 3.7 GHz.

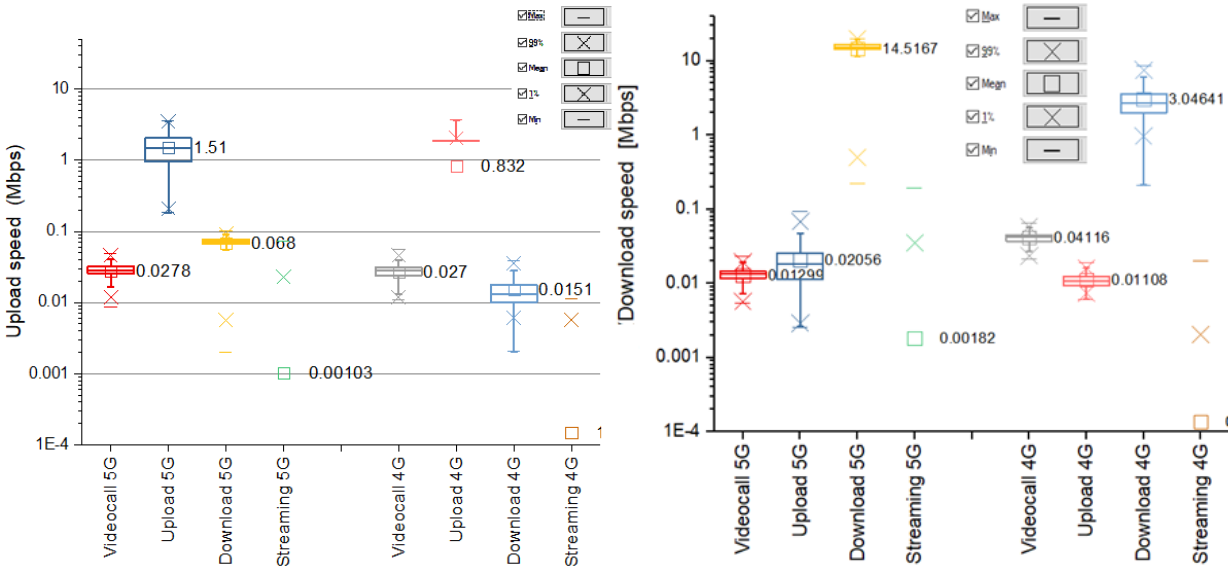

(a) (b)

Figure 10. Boxplots of data rates for 4G and 5G for: a) upload transfer; b) download transfer.

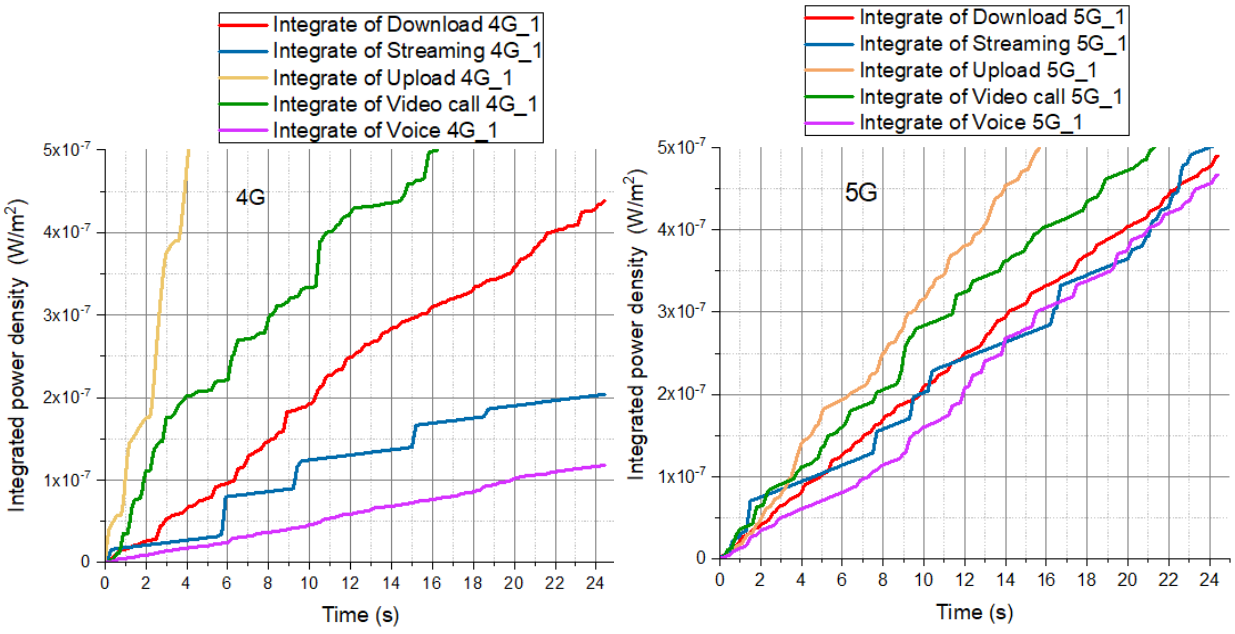

(a) **(b)**

Figure 11. Integrated power density as accumulated in air at 10 cm from the phone in 25 seconds of use: a) 4G applications; b) 5G applications.

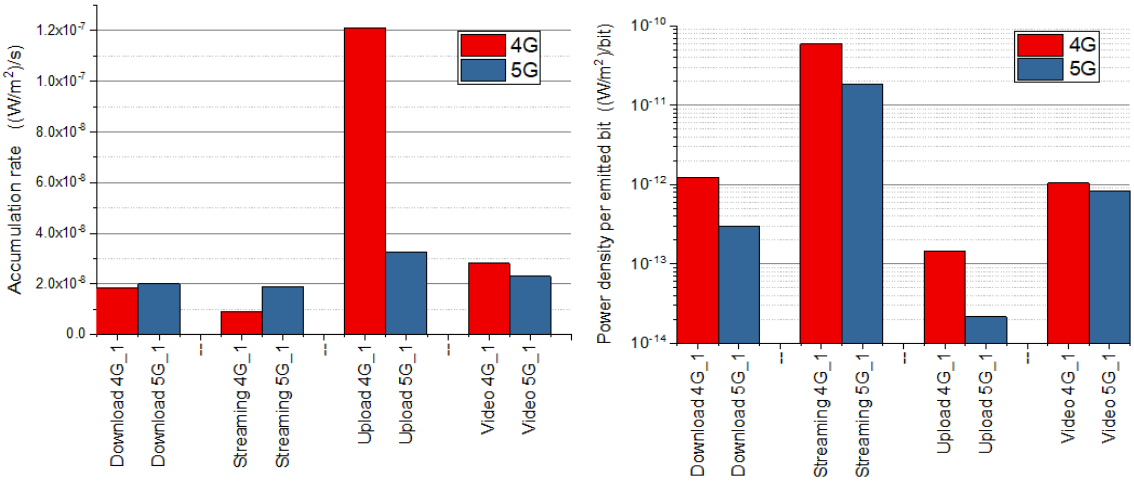

(a) **(b)**

Figure 12. a) Average rate of incident power density accumulation in air for 4G and 5G applications running over 24.5 s; b) Average rate of power density emitted per transferred bit in each situation.

5. Conclusions

Testing the peculiarities of human exposure to mobile terminal emissions in real-usage conditions, when the phone is connected to either 4G or 5G networks, was here approached for the first time. Using three synchronized real-time portable spectrum analysers connected to miniature E-field probes allowed experimental extraction of the rules by which the quasi-stochastic field levels are spread in time, during

the use of various data transfer or voice applications. The sample rate of collecting the received power data was 100 ms. The raw data were in the form of the spectrograms (matrices of 440 x 250), from which the channel power variation in time was computed. The transposed values were the absolute E-field strengths emitted during 25 s of monitoring. In parallel, by using a mobile application, synchronized information about the mean transferred data rates was gathered. The same mobile phone was used to connect to the same located base stations belonging to either 4G network or to 5G network. In 4G, the uplink channel was centred on 2.59 GHz and had a bandwidth of 20 MHz, while in pre-5G the channel was centred on 3.7 GHz and had a bandwidth of 40 MHz. The following peculiarities have been extracted:

- E-field strengths measured in air at 10 cm distance from the phone's surface were, on average, 31.7 % lower in 5G than in 4G, for all the checked applications: file upload, file download, streaming, video call and voice call.
- File upload provided the highest and the most spread values of the emitted field in both communication standards.
- Time variability of the emitted field was different for 4G and 5G emissions in all cases.
- The rate of power density accumulation in air, in the point of measurement, was lower in 5G than in 4G for all running applications, showing larger differences in 4G, in function of the mobile application used.
- Another interesting observation was related to the calculation of the average power density emitted per bit of transferred data: for all mobile applications, lower values of this indicator were obtained in 5G standard than in 4G.

Even if the data rates were not exceedingly higher in the 5G network, the time- and frequency-peculiarities of the in-air emitted field could be captured and quantified. Future work will be devoted to the follow-up of the changes that will be due to the full development of the 5G networks functionality from the point of view of the user exposure assessment due to his own mobile device.

Acknowledgments

This work was partially funded by the project no. PN-III-P1-1.1-PD-2019-0500 granted by CNCS – UEFISCDI Agency of the Romanian Ministry of Education and Research.

Conflict of interest

The authors declare that there is no conflict of interest.

References

1. TS 38-101.1: NR. User Equipment (UE) radio transmission and reception. Part 1: Range 1 Standalone, (17.2.0 ed.), 3GPP, 2021-07-09.
2. TS 38-101.2: NR. User Equipment (UE) radio transmission and reception. Part 2: Range 2 Standalone, (17.2.0 ed.), 3GPP, 2021-07-07.

3. 3GPP specification series: 38series. Retrieved August 5, 2021. Available from: https://www.3gpp.org/DynaReport/38-series.html
4. Miclaus S, Bechet P, Helbet R, et al. (2021) Towards 5G exposimetry: instantaneous and average energy density accumulation rate in air near wireless devices transmitting data as sub-millisecond frames. *2021 12th International Symposium on Advanced Topics in Electrical Engineering (ATEE)*, 1–4. https://doi.org/10.1109/ATEE52255.2021.9425087
5. Miclaus S, Sarbu A, Bechet P (2021) Using Poincare plots for feature extraction of the dynamics of electromagnetic field exposures when using different protocols of WiFi communications. *Proceedings of the 8th International Conference of Wireless Communication and Sensor Networks*, 32–38. https://doi.org/10.1145/3461717.3461723
6. Sarbu A, Miclaus S, Digulescu A, Bechet P (2020) Comparative analysis of user exposure to the electromagnetic radiation emitted by the 4th and 5th generations of Wi-Fi communication devices. *Int J Env Res Pub He* 17: 1–21. https://doi.org/10.3390/ijerph17238837
7. Miclaus S, Bechet P (2020) Non-stationary statistics with amplitude probability density function for exposure and energy density reporting nearby a mobile phone running 4G applications. *PIER M* 89: 151–159. https://doi.org/10.2528/PIERM19110706
8. ICNIRP (2020) Guidelines for limiting exposure to time-varying electric, magnetic, and electromagnetic fields (up to 300 GHz). *Health Phys* 118: 483–524.
9. IEEE-C95.1. (2019) IEEE standard for safety levels with respect to human exposure to radio frequency electromagnetic fields, 3 kHz to 300 GHz. Ed. NY, USA: IEEE.
10. IEC TR 63170:2018. Measurement procedure for the evaluation of power density related to human exposure to radio frequency fields from wireless communication devices operating between 6 GHz and 100 GHz.
11. Franci D, Coltellaci S, Grillo E, et al. (2020) Experimental procedure for fifth generation (5G) electromagnetic field (EMF) measurement and maximum power extrapolation for human exposure assessment. *Environments* 7: 22. https://doi.org/10.3390/environments7030022
12. Migliore MD, Franci D, Pavoncello S, et al. (2021) A new paradigm in 5G maximum power extrapolation for human exposure assessment: forcing gNB traffic toward the measurement equipment. *IEEE Access* 9: 101946–101958. https://doi.org/10.1109/ACCESS.2021.3092704
13. Velghe M, Aerts S, Martens L, et al. (2021) Protocol for personal RF-EMF exposure measurement studies in 5th generation telecommunication networks. *Environ Health* 20: 1–10. https://doi.org/10.1186/s12940-021-00719-w
14. Chitra S, Ramesh S, Jackson B, et al. (2020) Performance enhancement of generalized frequency division multiplexing with RF impairments compensation for efficient 5G wireless access. AEU - *International Journal of Electronics and Communications* 127: 153467. https://doi.org/10.1016/j.aeue.2020.153467
15. Velghe M, Shikhantsov S, Tanghe E, et al. (2020) Field enhancement and size of radio-frequency hotspots induced by maximum ratio field combining in fifth generation network. *Radiat Prot Dosimetry* 16: 400–411. https://doi.org/10.1093/rpd/ncaa118
16. Wang H, Xu B, Yao Y, et al. (2020) Implications of incident power density limits on power and EIRP levels of 5G millimeter-wave user equipment. *IEEE Access* 8: 148214–148225. https://doi.org/10.1109/ACCESS.2020.3015231

17. Joshi P, Ghasemifard F, Colombi D, et al. (2020) Actual output power levels of user equipment in 5G commercial networks and implications on realistic RF EMF exposure assessment. *IEEE Access* 8: 204068–204075. https://doi.org/10.1109/ACCESS.2020.3036977
18. Chiaraviglio L, Di Paolo C, Blefari Melazzi N (2021) 5G Network planning under service and EMF constraints: formulation and solutions. *IEEE Trans Mobile Comp*. https://doi.org/10.1109/TMC.2021.3054482
19. Lundgren J, Helander J, Gustafsson M, et al. (2019) Near-field measurement and calibration technique for RF EMF exposure assessment of mm-wave 5G devices. *IEEE Antennas Propag Mag*.
20. Lundgren J, Helander J, Gustafsson M, et al. (2021) A near-field measurement and calibration technique: radio-frequency electromagnetic field exposure assessment of millimeter-wave 5G devices. *IEEE Antennas Propag Mag* 63: 77–88. https://doi.org/10.1109/MAP.2020.2988517
21. He W, Scialacqua L, Scannavini A, et al. (2020) Incident power density assessment study for 5G millimeter-wave handset based on equivalent currents method. *Proceedings of 14th European Conference on Antennas and Propagation (EuCAP)*, 1–4. https://doi.org/10.23919/EuCAP48036.2020.9135622
22. He W, Xu B, Scialacqua L, et al. (2021) Fast power density assessment of 5G mobile handset using equivalent currents method. *IEEE T Antenn Propag* 69: 6857–6869. https://doi.org/10.1109/TAP.2021.3070725
23. Yazdandoost KY, Laakso I (2018) Numerical modeling of electromagnetic field exposure from 5G mobile communications at 10 GHz. *Progress in Electromagnetics Research* M 72: 61–67. https://doi.org/10.2528/PIERM18070503
24. Morelli MS, Gallucci S, Siervo B, et al. (2021) Numerical analysis of electromagnetic field exposure from 5G mobile communications at 28 GHZ in adults and children users for real-world exposure scenarios. *Int J Env Res Pub He* 18: 1073. https://doi.org/10.3390/ijerph18031073
25. Li K, Honda K (2021) A novel estimation method of local peak SAR for 5G sub-6GHz antennas using MIMO-OTA. *Proceedings of 15th European Conference on Antennas and Propagation (EuCAP)*, 1–3. https://doi.org/10.23919/EuCAP51087.2021.9411412
26. Zhekov SS, Zhao K, Franek O, et al. (2021) Test reduction for power density emitted by handset mmwave antenna arrays. *IEEE Access* 9: 23127–23138. https://doi.org/10.1109/ACCESS.2021.3055420
27. Cano R, Zhang S, Zhao K, et al. (2019) User body interaction of 5G switchable antenna system for mobile terminals at 28 GHz. *Proceedings of the European Conference on Antennas and Propagation (EuCAP)*.
28. Scialacqua L, Mioc F, Scannavini A, et al. (2020) Simulated and measured power density using equivalent currents for 5G applications. *IEEE International Symposium on Antennas and Propagation and North American Radio Science Meeting*, 1827–1828. https://doi.org/10.1109/IEEECONF35879.2020.9329619
29. Teniou M, Jawad O, Pannetrat S, et al. (2020) A fast and rigorous assessment of the specific absorption rate (SAR) for MIMO cellular equipment based on vector near-field measurements. *Proceedings of the 14th European Conference on Antennas and Propagation (EuCAP)*, 1–5. https://doi.org/10.23919/EuCAP48036.2020.9135506

30. Zhao K, Zhang S, Ho Z, et al. (2018) Spherical coverage characterization of 5G millimeter wave user equipment with 3GPP specifications. *IEEE Access* 7: 4442–4452. https://doi.org/10.1109/ACCESS.2018.2888981
31. Vanitha M, Ramesh S, Chitra S (2019) Wearable antennas for remote healthcare monitoring system using 5G wireless technologies. *Telecommunications and Radio Engineering* 78: 1275–1285. https://doi.org/10.1615/TelecomRadEng.v78.i14.50
32. Islam S, Zada M, Yoo H (2021) Low-pass filter based integrated 5G smartphone antenna for sub-6-GHz and mm-wave bands. *IEEE T Antenn Propag* 69: 1–13. https://doi.org/10.1109/TAP.2021.3061012
33. Bridges M, Khalily M, Abedian M, et al. (2020) High isolation 8×8 MIMO antenna design for 5G sub-6 GHz smartphone applications. In *International Conference on UK-China Emerging Technologies (UCET)*, 1–4. https://doi.org/10.1109/UCET51115.2020.9205450
34. Ramachandran T, Faruque MRI, Siddiky AM, et al. (2021) Reduction of 5G cellular network radiation in wireless mobile phone using an asymmetric square shaped passive metamaterial design. *Sci Rep* 11: 1–22. https://doi.org/10.1038/s41598-021-82105-7
35. Gultekin DH, Siegel PH (2020) Absorption of 5G radiation in brain tissue as a function of frequency, power and time. *IEEE Access* 8: 115593–115612. https://doi.org/10.1109/ACCESS.2020.3002183
36. Foster KR, Ziskin MC, Balzano Q, et al. (2021) Transient thermal responses of skin to pulsed millimeter waves. *IEEE Access* 8: 130239–130251. https://doi.org/10.1109/ACCESS.2020.3008322
37. Chiaraviglio L, Rossetti S, Saida S, et al. (2021) Pencil beamforming increases human exposure to electromagnetic fields: true or false? *IEEE Access* 9: 25158–25171. https://doi.org/10.1109/ACCESS.2021.3057237
38. Buda A, Sarbu A (2021) Development of an Android application for user exposure assessment to electromagnetic fields emitted by an IEEE 802.11ax client. *Proceedings of the IEEE International Black Sea Conference on Communications and Networking*. https://doi.org/10.1109/BlackSeaCom52164.2021.9527788
39. Bechet P, Miclaus S, Bechet AC (2015) An analysis of the dependence of the electromagnetic exposure level in indoor environment on traffic direction, instantaneous data rate and position of the devices in a WLAN network. *Measurement*, 67: 34–41. https://doi.org/10.1016/j.measurement.2015.02.035

AIMS Press